

NBBOX: Noisy Bounding Box Improves Remote Sensing Object Detection

Yechan Kim^{ID}, *Student Member, IEEE*, SooYeon Kim^{ID}, *Student Member, IEEE*, and
Moongu Jeon^{ID}, *Senior Member, IEEE*

Abstract—Data augmentation has seen significant advancements in computer vision to improve model performance over the years, particularly in scenarios with limited and insufficient data. Currently, most studies focus on adjusting the image or its features to expand the size, quality, and variety of samples during training in various tasks including object detection. However, we argue that it is necessary to investigate bounding box transformations as a model regularization technique rather than image-level transformations, especially in aerial imagery due to potentially inconsistent bounding box annotations. Hence, this letter presents a thorough investigation of bounding box transformation in terms of scaling, rotation, and translation for remote sensing object detection. We call this augmentation strategy NBBOX (Noise Injection into Bounding Box). We conduct extensive experiments on DOTA and DIOR-R, both well-known datasets that include a variety of rotated generic objects in aerial images. Experimental results show that our approach significantly improves remote sensing object detection without whistles and bells and it is more time-efficient than other state-of-the-art augmentation strategies.

Index Terms—Noisy bounding box, oriented bounding box, remote sensing object detection, data augmentation.

I. INTRODUCTION

IN recent years, remote sensing object detection has achieved remarkable success primarily due to the advancements in deep learning. Particularly, modern deep learning architectures such as convolutional neural networks and transformers have significantly enhanced the capabilities of object detection in Earth vision. These models have millions or billions of parameters to learn, requiring tremendous training data to avoid the over-fitting problem. Compared to natural scenes (e.g. ImageNet [1] or MS-COCO [2]), datasets for overhead imagery usually lack diversity and quantity due to the expense of data collection. To overcome this limitation, data augmentation plays a significant role as an implicit regularization strategy for model learning.

Existing visual data augmentation methods can be mainly divided into three categories: (a) image manipulation (e.g. [3], [4], [5], [6]), (b) feature transformation (e.g. [7], [8]), and (c) generative image synthesis (e.g. [9], [10], [11]). For (a), geometric transformations (such as flipping and shearing),

sharpness transformations, noise distribution, etc are considered the simplest augmentations. More advanced strategies in image manipulation contain image erasing and image mix. The image erasing like [3], [4] randomly selects a sub-region in an image and deletes its contents, while the image mix like [5], [6] combines two or more images (or patches) as a single image during training. Meanwhile, (b) aims to directly manipulate features in the latent space rather than that raw input image. For example, [7] applies augmentations to the extracted features and encourages the model to be consistent for both the original and augmented features. [8] leverages the synergy between feature normalization and data augmentation to improve the robustness and accuracy of models. Unfortunately, both are hard to directly apply to rotated object detection. Finally, (c) produces samples with generative models based on GAN [9] or Diffusion [11]. Such methods can generate high-quality (for GAN) or high-fidelity (for Diffusion) samples, but these require significant computational resources.

While most prior work for data augmentation concentrates on adjusting the image or its features, only few have focused on the deformation of bounding boxes for object detection. However, [12] discovers the presence of low-confidence annotations in current overhead object detection datasets: there is a mismatch between the minimum enclosing box (i.e. optimal) and the actual annotation. Thus, we argue that investigating bounding box transformation is necessary to boost the model performance for remote sensing object detection, by enabling robust training in potentially inaccurate bounding boxes.

In this letter, we propose a simple but efficient data augmentation method named NBBOX (Noise Injection into Bounding Box) for remote sensing object detection. Intuitively, our method adds noise to bounding boxes with geometric transformations during training (not for test/deployment). Particularly, this work thoroughly investigates bounding box transformation in terms of scaling, rotation, and translation. To demonstrate the effectiveness of our approach, extensive experiments are conducted on DOTA [13] and DIOR-R [14], both datasets that contain rotated and densely-placed objects.

The main contributions of this work are as follows:

- To the best of our knowledge, we first investigate the bounding box transformation to improve remote sensing object detection. With our investigation, we provide a useful recipe for adding noise to bounding boxes.
- It is worth noting that our method is easy to plug in and merely increases the computational complexity compared to other state-of-the-art data augmentation strategies.
- Extensive experimental results demonstrate that NBBOX can boost remote sensing object detection without whistles and bells, against implicit box label noise.

Manuscript received September 00, 2024; accepted 0000000000 00, 0000. Date of publication 0000000000 00, 0000; date of current version 0000000000 00, 0000. This work was supported by the Agency For Defense Development Grant funded by the Korean Government (UI220066WD). (Corresponding author: Moongu Jeon.)

Yechan Kim, SooYeon Kim, and Moongu Jeon are with the School of Electrical Engineering and Computer Science, Gwangju Institute of Science and Technology (GIST), Gwangju 61005, South Korea (e-mail: yechankim@gm.gist.ac.kr, bluesooyeon@gm.gist.ac.kr, mgjeon@gist.ac.kr).

This article has supplementary downloadable material available at <https://ieeexplore.ieee.org/>, provided by the authors.

Digital Object Identifier 10.XXXX/XXXX.2024.0000000

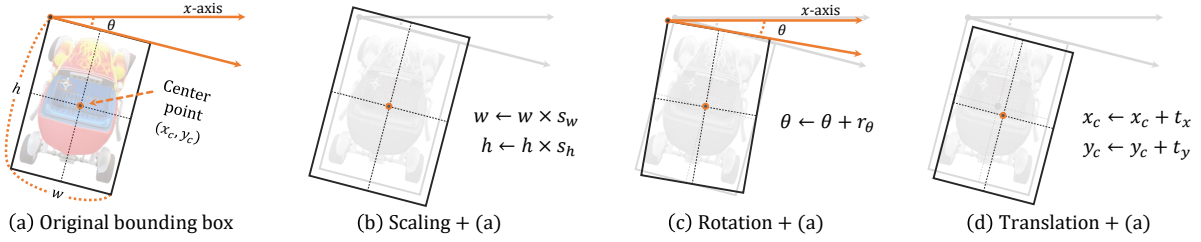


Fig. 1. Examples of the proposed data augmentation method named **NBBOX** for remote sensing object detection.

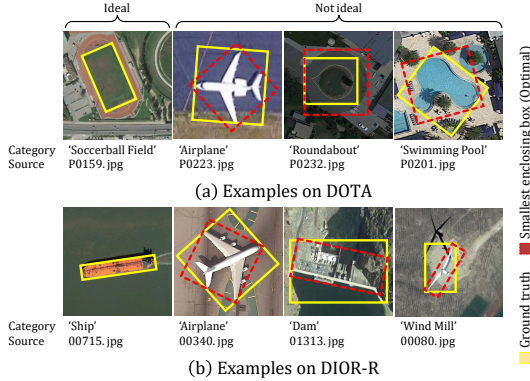


Fig. 2. Comparison between provided bounding box labels and minimum enclosing rectangles for objects on DOTA and DIOR-R.

II. METHODOLOGY

In this section, we present a simple, but efficient data augmentation strategy namely **NBBOX** (**N**oise **I**njection into **B**ounding **B**ox) for remote sensing object detection. Our method can be easily integrated into existing detection frameworks with minimal modifications. More precisely, our augmentation method can be seamlessly added to any data pre-processing pipeline without severe computational burden. The proposed approach is straightforward as depicted in Fig. 1. For data augmentation, our training scheme randomly adds noise to oriented bounding boxes with the three simplest geometric transformations: scaling, rotation, and translation.

A. Background

Training models under label noise is challenging and requires careful consideration to learn resilient and generalized models. Most research attention has been given to the classification task, but recently a few have dedicated to object detection (e.g. [15], [16], [17], [18] for natural scenes and [19], [20], [21] for remote sensing imagery).

For natural images, [15] first analyzes the effects of various label noise types on object detection and introduces a per-object co-teaching framework to address the noise label issue. [16] suggests a learning strategy of alternating between rectifying noise and training the model to handle label noise concerning category and bounding box. [17] proposes to address label noise by adopting meta-learning via exploiting a few clean labels. Previous studies consider classification and localization simultaneously, whereas [18] employs multiple instance learning to deal solely with inaccurate bounding boxes. We believe that it is reasonable and practical to pursue

this research direction as imprecise bounding box labels are more prevalent than noisy category labels in practice.

For remote sensing images, a few work has been proposed to address noisy labels in object detection, inspired by research for natural scenes. As seen in Fig. 2, there is a discrepancy between the actual annotation and the minimum enclosing box, which might cause difficulties in model training due to inaccurate and low-consistent bounding boxes. [19] designs two kinds of loss functions to mitigate mislabels for both classification and localization. On the other hand, [20], [21] focus on correcting incomplete annotations such as missing bounding boxes due to misalignment of GPS sensors. The main goal of our work is to resolve localization errors inherent in the existing bounding box labels. In other words, we consider a generic object detection scenario, where missing bounding boxes or incorrect class labels of the ground truth are uncommon. Instead, we assume that the bounding box labels may not be optimal due to the annotators' mistakes or dilemma situations such as how to rotate a bounding box for a circular object on overhead imagery during the annotation process. In particular, we study a data augmentation strategy based on bounding box transformation for more robust localization.

B. Overview of the proposed approach

The detail of **NBBOX** is presented in Algorithm 1. In our algorithm, there exist two types of input: \mathbf{I} is the input image and $\mathbf{L} = \{(\mathbf{B}_i, \mathbf{c}_i)\}_{i=1}^N$ is the corresponding labels of N objects for object detection, where $\mathbf{B}_i = (x_c, y_c, w, h, \theta)$ and \mathbf{c}_i correspond to the bounding box label and the one-hot encoded category label for i -th object, respectively. (x_c, y_c) is the center point, while w and h represent the width and height of the bounding box. θ denotes the rotated angle of the box.

Moreover, there are three kinds of hyper-parameters to tune. $\mathbf{s} = (s_{\min}, s_{\max})$, $\mathbf{r} = (r_{\min}, r_{\max})$, and $\mathbf{t} = (t_{\min}, t_{\max})$ determine the ranges of translation, scaling, and rotation, respectively, where $\forall k, s_k \in \mathbb{R} \wedge r_k \in \mathbb{R} \wedge t_k \in \mathbb{Z}$. Here, \mathbb{Z} is the set of all integers whereas \mathbb{R} is for all real numbers.

$\text{rand}_{\text{int}}(a, c) \sim P_{\text{int}}$ selects and returns any specific integer c such that $a \leq b \leq c$. $\text{rand}_{\text{float}}(a, c) \sim P_{\text{float}}$ generates any real number value within the closed interval $[a, c]$. We simply choose the uniform distributions for all random functions used in our algorithm. In other words, $P(b; a, c) = \frac{1}{c-a+1}$ and $P(b; a, c) = \frac{1}{c-a}$ are used for the probability mass (discrete) function P_{int} and the probability density (continuous) function P_{float} , respectively. One might question why \mathbf{t} has a domain of integer values while \mathbf{s} and \mathbf{r} have domains of real numbers. This is because translation operations are conducted on a pixel basis, while scaling and rotation factors can be the real number.

Algorithm 1: Procedure of NBBOX.

Input : Input image \mathbf{I} , Labels $\mathbf{L} = \{(\mathbf{B}_i, \mathbf{c}_i)\}_{i=1}^N$
Parameters: Scaling range $\mathbf{s} = (s_{\min}, s_{\max})$,
Rotation range $\mathbf{r} = (r_{\min}, r_{\max})$,
Translation range $\mathbf{t} = (t_{\min}, t_{\max})$
Output : Input image \mathbf{I} , Updated labels \mathbf{L}^*

```

1 for  $i \leftarrow 1$  to  $N$  do
2    $x_c, y_c, w, h, \theta \leftarrow \mathbf{B}_i$ ;
3   // (1) BBOX Scaling
4    $s_w, s_h \leftarrow \text{rand}_{\text{float}}(s_{\min}, s_{\max}), \text{rand}_{\text{float}}(s_{\min}, s_{\max})$ ;
5    $w^*, h^* \leftarrow w \times s_w, h \times s_h$ ;
6   // (2) BBOX Rotation
7    $r_\theta \leftarrow \text{rand}_{\text{float}}(r_{\min}, r_{\max})$ ;
8    $\theta^* \leftarrow \theta + r_\theta$ ;
9   // (3) BBOX Translation
10   $t_x, t_y \leftarrow \text{rand}_{\text{int}}(t_{\min}, t_{\max}), \text{rand}_{\text{int}}(t_{\min}, t_{\max})$ ;
11   $x_c^*, y_c^* \leftarrow x_c + t_x, y_c + t_y$ ;
12  // Update
13   $\mathbf{B}_i^* \leftarrow x_c^*, y_c^*, w^*, h^*, \theta^*$ ;
14  $\mathbf{L}^* \leftarrow \{(\mathbf{B}_i^*, \mathbf{c}_i)\}_{i=1}^N$ ;

```

Assume that a single image \mathbf{I} is given with labels \mathbf{L} to our algorithm. The ultimate goal is to perform bounding box transformations during training as a data augmentation strategy. To clarify, we randomly add noise to each bounding box \mathbf{B}_i in \mathbf{L} for each training epoch. In Algorithm 1, for each box \mathbf{B}_i , three kinds of transformations are applied in sequence (scaling: line 4-5, rotation: line 7-8, translation: line 10-11). Note that it is possible to activate only a subset of these sub-operations during the execution of **NBBOX**. For instance, you can simply choose not to use ‘rotation’ for **NBBOX** if needed.

C. Advanced options for translation and scaling

As demonstrated in Algorithm 1, the bounding box may be translated by different values along both the x-axis and y-axis. Besides, the aspect ratio may not be maintained for scaling operations. This phenomenon would not be recommended for training on certain data scenarios. For instance, it would not be desirable to modify the aspect ratio of bounding boxes in an extreme situation where most objects are expected to have a square size. Hence, we alleviate this by providing additional parameters $\text{bool}_s \in \{\text{True}, \text{False}\}$ and $\text{bool}_t \in \{\text{True}, \text{False}\}$ in our **NBBOX** algorithm. Here, bool_s and bool_t are boolean values to be set by users. One can effortlessly modify our algorithm with bool_s and bool_t as follows.

For scaling, line 4 should be replaced with:

$$\begin{aligned} \alpha, \beta &\leftarrow \text{rand}_{\text{float}}(s_{\min}, s_{\max}), \text{rand}_{\text{float}}(s_{\min}, s_{\max}); \\ s_w &\leftarrow \alpha \text{ if } \text{bool}_s \text{ is True, otherwise } \alpha; \\ s_h &\leftarrow \alpha \text{ if } \text{bool}_s \text{ is True, otherwise } \beta, \end{aligned} \quad (1)$$

where bool_s represents whether the bounding box is proportionally resized to keep the width and height ratio unchanged.

Likewise, for translation, line 10 should be replaced with:

$$\begin{aligned} \alpha, \beta &\leftarrow \text{rand}_{\text{int}}(t_{\min}, t_{\max}), \text{rand}_{\text{int}}(t_{\min}, t_{\max}); \\ t_x &\leftarrow \alpha \text{ if } \text{bool}_t \text{ is True, otherwise } \alpha; \\ t_y &\leftarrow \alpha \text{ if } \text{bool}_t \text{ is True, otherwise } \beta, \end{aligned} \quad (2)$$

where bool_t denotes whether the center point is shifted equally along both the x and y directions.

III. EXPERIMENTS

In this section, we show our data augmentation strategy **NBBOX** improves the performance of remote sensing object detection. We first briefly introduce the experimental settings and implementation details. We then provide test results and analysis of experiments with the proposed method.

A. Experimental setup

Detection models. Traditionally, deep learning-based object detection models are typically separated into one-stage and two-stage methods. Nowadays, the distinction between anchor-based and anchor-free methodologies tends to be more emphasized when classifying detector models. In this work, we adopt Faster R-CNN [22], RetinaNet [23], and FCOS [24] which are representative models in anchor-based two-stage, anchor-based one-stage, and anchor-free one-stage detection studies, respectively. For all models, Imagenet-pretrained ResNet-50 [25] is used for feature extraction, and FPN-1x [26] is added as a neck to improve multi-scale invariance.

Training details. We implement our hypothesis using PyTorch and MMRotate [27]. All the models are trained for 25 epochs. For a fair comparison with other approaches, all the experiments are resumed with weights pre-trained for five epochs without any augmentation per each {detector, data} combination. SGD is used for optimization with momentum of weight 0.9, weight decay $1e-4$, learning rate $1e-3$, and batch size 8. Learning rate warm-up is used over the first 500 iterations, where the learning rate linearly increases from zero to 33% of $5e-3$. L2-norm gradient clipping is utilized with a maximum norm of 35. We apply the following pre-processing operations for training: ‘RResize’, ‘RRandomFlip’, ‘Normalize’, and ‘Pad’, while for testing, ‘MultiScaleFlipAug’ is also used. For the sake of brevity and due to time limitations, we only conduct the parameter search on DIOR-R and scale the best configurations to DOTA in this work.

Evaluation metric. To objectively verify performance, all experiments are repeated five times, and the evaluation results are reported as ‘mean \pm standard deviation’. For each experiment, we use mAP (mean Average Precision) at $\text{IoU}(\hat{\mathbf{y}}, \mathbf{y})=0.5$ (i.e. mAP@50) to measure the accuracy of the detected bounding boxes ($\hat{\mathbf{y}}$) against the ground truth boxes (\mathbf{y}) following [2]. This metric evaluates both the precision and recall of the model across different classes as:

$$\text{mAP} = \frac{1}{C} \sum_{i=1}^C \text{AP}_i, \quad (3)$$

where C is the number of categories and AP_i is the average precision for category i . See [28] for detailed calculation.

B. Datasets

This work conducts experiments on two widely recognized datasets for remote sensing object detection: DOTA (v1) [13] and DIOR-R [14]. Both have diverse real-world categories, high resolution, and detailed annotations. DOTA includes 15 object categories such as ‘car’, ‘ship’, and ‘harbor’. It contains 2,806 aerial images of varying resolutions with 188,282 oriented bounding box labels. Compared to DOTA, DIOR-R has 20 object categories including 192,512 instances over 23,463 images for rotated object detection. We conduct experiments

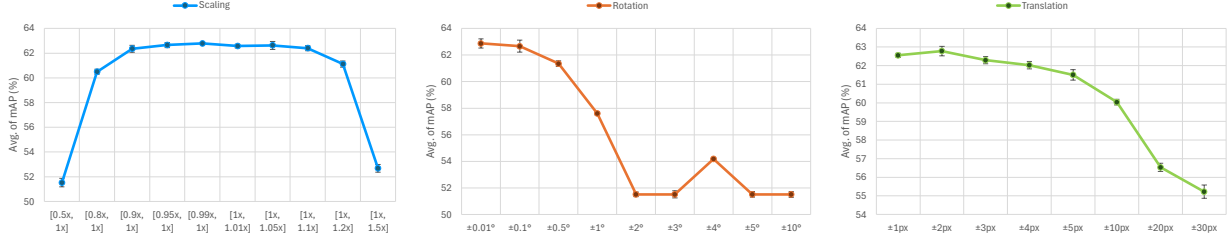


Fig. 3. Impact of scaling, rotation, and translation of bounding boxes on model performance: as we observe similar outcomes across different architectures and datasets, for brevity, we include only the result from Faster R-CNN trained on DIOR-R.

TABLE I

EXPERIMENTAL RESULTS OF SCALING, ROTATION, AND TRANSLATION OF BOUNDING BOXES ACROSS VARIOUS DETECTION ARCHITECTURES ON DIOR-R WITH **NBBOX**. (**BOLD** TEXT MEANS THE BEST WHILE UNDERLINED AND WAVY-UNDERLINED TEXT INDICATE THE SECOND- AND THIRD-BEST, RESPECTIVELY IN THIS WORK)

Configuration				Detectors		
Transform	s_{\min} (r_{\min}) < t_{\min} >	s_{\max} (r_{\max}) < t_{\max} >	$bool_s$ < $bool_t$ >	Faster R-CNN	FCOS	RetinaNet
Scaling	0.5x	1x	True	51.52 ± 0.34	42.17 ± 1.04	36.92 ± 0.36
			False	51.52 ± 0.34	43.41 ± 1.17	37.90 ± 0.88
	0.8x	1x	True	60.49 ± 0.21	58.50 ± 0.88	54.48 ± 0.60
			False	60.52 ± 0.45	58.52 ± 1.03	54.10 ± 1.02
	0.9x	1x	True	62.36 ± 0.28	59.60 ± 1.01	55.46 ± 0.72
			False	62.39 ± 0.22	59.39 ± 0.76	55.06 ± 0.68
	0.95x	1x	True	<u>62.66 ± 0.20</u>	<u>59.78 ± 0.78</u>	<u>55.60 ± 0.65</u>
			False	62.45 ± 0.11	59.58 ± 0.92	55.77 ± 0.82
	0.99x	1x	True	<u>62.79 ± 0.05</u>	<u>60.00 ± 0.99</u>	<u>55.50 ± 0.55</u>
			False	62.65 ± 0.18	59.74 ± 1.13	55.31 ± 0.85
	1x	1.01x	True	<u>62.57 ± 0.14</u>	<u>59.91 ± 0.86</u>	<u>55.79 ± 0.72</u>
			False	62.71 ± 0.27	59.68 ± 1.09	55.74 ± 0.47
	1x	1.05x	True	62.63 ± 0.32	59.68 ± 0.99	55.64 ± 0.75
			False	62.28 ± 0.09	59.55 ± 1.12	55.40 ± 0.78
1x	1.1x	True	62.41 ± 0.21	59.56 ± 1.15	55.33 ± 0.70	
		False	62.12 ± 0.21	59.48 ± 0.97	55.44 ± 0.62	
1x	1.2x	True	61.12 ± 0.24	58.77 ± 0.99	54.64 ± 0.69	
		False	61.03 ± 0.22	58.58 ± 0.95	54.60 ± 0.75	
1x	1.5x	True	52.68 ± 0.32	51.72 ± 1.14	48.38 ± 0.84	
		False	53.12 ± 0.21	51.28 ± 0.90	48.17 ± 0.80	
Rotation	-0.01°	0.01°	-	<u>62.87 ± 0.29</u>	<u>59.68 ± 1.03</u>	<u>55.40 ± 0.53</u>
	-0.1°	0.1°	-	62.66 ± 0.15	59.66 ± 1.03	55.37 ± 0.90
	-0.5°	0.5°	-	61.35 ± 0.21	58.46 ± 0.91	54.40 ± 0.99
	-1°	1°	-	57.60 ± 0.26	54.16 ± 0.73	52.23 ± 0.41
	-2°	2°	-	51.52 ± 0.34	37.95 ± 3.70	32.72 ± 2.23
	-3°	3°	-	51.52 ± 0.34	39.04 ± 2.08	37.59 ± 0.53
	-4°	4°	-	54.19 ± 0.27	47.85 ± 0.42	51.79 ± 0.85
	-5°	5°	-	51.52 ± 0.34	38.88 ± 2.26	37.94 ± 0.42
	-10°	10°	-	51.52 ± 0.34	43.44 ± 0.44	48.73 ± 0.23
	<Translation>	-1px	1px	True	62.56 ± 0.12	<u>59.93 ± 0.91</u>
False				62.73 ± 0.25	59.70 ± 0.95	55.42 ± 0.58
-2px		2px	True	<u>62.78 ± 0.26</u>	<u>59.72 ± 0.92</u>	55.33 ± 0.69
			False	62.59 ± 0.25	<u>59.75 ± 1.02</u>	55.45 ± 0.90
-3px		3px	True	62.30 ± 0.19	59.62 ± 1.19	55.51 ± 0.61
			False	62.56 ± 0.14	59.71 ± 0.88	55.69 ± 0.60
-4px		4px	True	62.03 ± 0.20	59.46 ± 1.27	55.35 ± 0.70
			False	61.73 ± 0.22	59.14 ± 1.39	55.48 ± 0.66
-5px		5px	True	61.51 ± 0.28	59.49 ± 1.31	55.34 ± 0.74
			False	61.78 ± 0.11	58.82 ± 1.41	55.39 ± 0.69
-10px		10px	True	60.04 ± 0.15	58.33 ± 1.30	54.36 ± 1.08
			False	59.23 ± 0.27	57.31 ± 1.37	53.99 ± 0.73
-20px		20px	True	56.53 ± 0.22	56.15 ± 1.09	51.22 ± 1.05
			False	52.17 ± 0.16	52.14 ± 0.99	48.88 ± 0.76
-30px	30px	True	55.23 ± 0.36	54.30 ± 1.34	49.96 ± 0.64	
		False	51.52 ± 0.34	48.77 ± 0.88	45.81 ± 0.81	

and report results based on the standard convention like [29] in the remote sensing community for both datasets.

C. Impact of scaling, rotation, and translation in **NBBOX**

This subsection studies the model performance when exposed to varying levels of scaling, rotation, and translation of bounding boxes. For this, we consider combinations of the following parameters: $s_{\min} \in \{0.5, 0.8, 0.9, 0.95, 0.99\}$, $s_{\max} \in \{1, 1.01, 1.05, 1.1, 1.2, 1.5\}$, $bool_s \in \{\text{True}, \text{False}\}$, $\{r_{\min}, r_{\max}\} \in \{\pm 0.01, \pm 0.1, \pm 0.5, \pm 1, \pm 2, \pm 3, \pm 4, \pm 5, \pm 10\}$, and $\{t_{\min}, t_{\max}\} \in \{\pm 1, \pm 2, \pm 3, \pm 4, \pm 5, \pm 10, \pm 20, \pm 30\}$, $bool_t \in \{\text{True}, \text{False}\}$. As indicated in Fig. 3 and Table I, following hyper-parameters are recommended:

- $s_{\min} \in \{0.95, 1\} \wedge s_{\max} \in \{1, 1.01\}$;
- $\{r_{\min}, r_{\max}\} = \{\pm 0.01\}$ & $t_{\min} = \pm 1, t_{\max} = \pm 2$.

For rotation, we need to use fairly small parameter values, presumably as rotating bounding boxes can easily harm foreground content in aerial imagery, especially for tiny objects.

Isotropic scaling and translation. When scaling with preserving aspect ratio (i.e. $bool_s = \text{True}$), all models show a slight increase in mAP compared to when it is not (i.e. $bool_s = \text{False}$) as shown in Table II. Besides, in the case of translation noise, the models perform slightly better when isotropic translation is applied (i.e. $bool_t = \text{True}$) compared to when it is not (i.e. $bool_t = \text{False}$) as indicated in Table II. Thus, experimental results on DIOR-R in Table II suggest that isotropic scaling and translation may be important. However, it is vital to note that the performance observed in this experiment might not be consistently replicable across different datasets.

TABLE II
AVERAGE MAP UNDER ISOTROPIC/NON-ISOTROPIC SCALING AND TRANSLATION NOISES FOR EACH PARAMETERS (s_{\min} , s_{\max} , t_{\min} , AND t_{\max}) ON DIOR-R IN **NBBOX**.

Configuration		Faster RCNN	FCOS	RetinaNet
Scaling	$bool_s = \text{True}$	60.12 (+0.05)	56.97 (+0.05)	52.77 (+0.03)
	$bool_s = \text{False}$	60.07	56.92	52.74
Translation	$bool_t = \text{True}$	60.37 (+1.08)	58.38 (+1.46)	54.10 (+0.83)
	$bool_t = \text{False}$	59.29	56.92	53.27

Combining scaling, rotation, and translation. There is a reasonable expectation that integrating scaling, rotation, and translation could synergistically improve the model's robustness and generalization. Hence, we further conduct experiments to validate the effectiveness of such combinations. Precisely, we study different combinations of each transformation (with parameters that show the best): pairwise combinations and the complete combination. Table III indicates the effectiveness of the combined transformations in enhancing the model's performance. Notably, the improvements are particularly evident in the scenario when we simultaneously use scaling, rotation, and translation during training.

TABLE III
IMPACT OF COMBINING SCALING, ROTATION, AND TRANSLATION OF BOUNDING BOXES ON DIOR-R IN **NBBOX**.

Transform	Faster R-CNN	FCOS	RetinaNet
Scaling (Best)	62.79 ± 0.05	60.00 ± 0.99	55.79 ± 0.72
Rotation (Best)	62.87 ± 0.29	59.68 ± 1.03	55.40 ± 0.53
Translation (Best)	62.78 ± 0.26	59.93 ± 0.91	55.71 ± 0.74
Scaling + Rotation	62.92 ± 0.24	60.13 ± 0.97	56.02 ± 0.65
Scaling + Translation	62.89 ± 0.30	60.02 ± 1.07	56.06 ± 0.65
Translation + Rotation	62.80 ± 0.22	59.89 ± 1.06	56.00 ± 0.72
Scaling + Rotation + Translation	63.18 ± 0.14	60.25 ± 1.00	56.09 ± 0.61

D. Comparison with state-of-the-art methods

In this subsection, we compare our method with easy-to-get data augmentation methods based on image manipulation (image/patch erasing and mix) as illustrated in Table IV. We also compare ours with RandRotate and RandShift to show the difference (Our method differs as it only transforms bounding boxes while RandRotate and RandShift rotate or shift both the image and the bounding boxes). For a DOTA dataset, we follow the best parameters across three detectors on DIOR-R by hard voting. Additionally, we train and test only on Faster R-CNN, the best architecture on DIOR-R in our previous experiments. Table IV shows that our **NBBOX** achieves the best performance among the state-of-the-art augmentation methods. Though our method, when applied solely to DOTA, achieved competitive performance, ranking second behind RandRotate, its performance significantly improves when integrated with RandRotate. Such is true of RetinaNet on DIOR-R with MosaicMix. Besides, our method is faster than other image manipulation methods. Table V indicates the time required per each training epoch on Faster R-CNN for each augmentation. (e.g. for one epoch, ours vs MosaicMix: 9.63min vs 21.24min on DIOR-R). Due to the page limit, detailed settings are described in the supplementary material.

TABLE IV
COMPARISON OF STATE-OF-THE-ART METHODS.

Data	DIOR-R			DOTA
	Faster R-CNN	FCOS	RetinaNet	Faster R-CNN
Baseline	62.66 ± 0.17	59.75 ± 1.09	55.69 ± 0.77	68.92 ± 0.44
+ RandRotate [30]	63.10 ± 0.21	60.11 ± 1.12	55.85 ± 0.87	70.02 ± 0.32
+ RandShift [30]	62.87 ± 0.37	59.67 ± 1.05	55.07 ± 0.83	69.01 ± 0.40
+ Cutout [3]	62.91 ± 0.26	59.84 ± 0.99	55.83 ± 0.92	69.13 ± 0.45
+ AutoAug [31]	62.33 ± 0.31	59.24 ± 1.07	54.78 ± 1.13	68.87 ± 0.32
+ RandAug [32]	62.55 ± 0.12	59.94 ± 1.29	55.17 ± 1.22	66.11 ± 0.24
+ AugMix [33]	62.83 ± 0.11	59.93 ± 0.75	55.74 ± 0.99	69.26 ± 0.10
+ MosaicMix [6], [34]	61.15 ± 0.19	58.03 ± 0.76	<u>56.15</u> ± 0.31	62.73 ± 0.58
+ YOCCO [35]	57.52 ± 0.16	54.37 ± 1.70	51.14 ± 1.01	65.16 ± 0.36
+ PixMix [36]	62.07 ± 0.23	58.91 ± 1.13	54.61 ± 0.74	68.72 ± 0.33
+ Ours (Best)	63.18 ± 0.14	60.25 ± 1.00	<u>56.09</u> ± 0.61	69.79 ± 0.35
+ Ours (Best) + RandRotate	-	-	-	70.36 ± 0.31
+ Ours (Best) + MosaicMix	-	-	56.32 ± 0.36	-

TABLE V
TIME ANALYSIS OF EACH TRANSFORMATION USED IN THIS WORK.

Detector: Faster R-CNN	DIOR-R	DOTA
RandRotate [30]	9.65min	17.12min
RandShift [30]	9.66min	16.37min
Cutout [3]	9.66min	16.29min
AutoAug [31]	9.70min	16.32min
RandAug [32]	9.64min	16.34min
AugMix [33]	9.75min	16.61min
MosaicMix [6], [34]	21.24min	34.48min
YOCCO [35]	9.77min	16.40min
PixMix [36]	9.75min	16.54min
Ours (Scaling + Rotation + Translation)	9.63min	16.28min

IV. CONCLUSION

In this letter, we have proposed a novel data augmentation method named **NBBOX** for remote sensing object detection. This work thoroughly investigates the effect of bounding box transformation with scaling, rotation, and translation for remote sensing object detection. Extensive experiments on DOTA and DIOR-R demonstrate that noise injection into bounding boxes surpasses existing state-of-the-art augmentation strategies based on image manipulation. Besides, **NBBOX** is easy to integrate with modern deep-learning frameworks and more time-efficient than other augmentation methods. In the future, we will extend our method with self-supervised learning such as multiple instance learning for further improvement.

REFERENCES

- [1] J. Deng *et al.*, “Imagenet: A large-scale hierarchical image database,” in *CVPR*, 2009.
- [2] T.-Y. Lin *et al.*, “Microsoft coco: Common objects in context,” in *ECCV*, 2014.
- [3] T. DeVries *et al.*, “Improved regularization of convolutional neural networks with cutout,” *arXiv preprint*, 2017.
- [4] Z. Zhong *et al.*, “Random erasing data augmentation,” in *AAAI*, 2020.
- [5] S. Yun *et al.*, “Cutmix: Regularization strategy to train strong classifiers with localizable features,” in *ICCV*, 2019.
- [6] R. Takahashi *et al.*, “Data augmentation using random image cropping and patching for deep cnns,” *IEEE Transactions on Circuits and Systems for Video Technology*, 2019.
- [7] C.-W. Kuo *et al.*, “Featmatch: Feature-based augmentation for semi-supervised learning,” in *ECCV*, 2020.
- [8] B. Li *et al.*, “On feature normalization and data augmentation,” in *CVPR*, 2021.
- [9] I. Goodfellow *et al.*, “Generative adversarial nets,” in *NeurIPS*, 2014.
- [10] J.-Y. Zhu *et al.*, “Unpaired image-to-image translation using cycle-consistent adversarial networks,” in *ICCV*, 2017.
- [11] B. Trabucco *et al.*, “Effective data augmentation with diffusion models,” *arXiv preprint*, 2023.
- [12] J. Murrugarra-Llerena *et al.*, “Can we trust bounding box annotations for object detection?,” in *CVPRW*, 2022.
- [13] G.-S. Xia *et al.*, “Dota: A large-scale dataset for object detection in aerial images,” in *CVPR*, 2018.
- [14] G. Cheng *et al.*, “Anchor-free oriented proposal generator for object detection,” *IEEE Transactions on Geoscience and Remote Sensing*, 2022.
- [15] S. Chadwick and P. Newman, “Training object detectors with noisy data,” in *IEEE IV*, 2019.
- [16] J. Li, C. Xiong, R. Socher, and S. Hoi, “Towards noise-resistant object detection with noisy annotations,” *arXiv preprint*, 2020.
- [17] Y. Xu *et al.*, “Training robust object detectors from noisy category labels and imprecise bounding boxes,” *IEEE Transactions on Image Processing*, 2021.
- [18] C. Liu *et al.*, “Robust object detection with inaccurate bounding boxes,” in *ECCV*, 2022.
- [19] S. Wei *et al.*, “Object detection with noisy annotations in high-resolution remote sensing images using robust efficientdet,” in *Image and Signal Processing for Remote Sensing*, 2021.
- [20] M. Bernhard *et al.*, “Correcting imprecise object locations for training object detectors in remote sensing applications,” *Remote Sensing*, 2021.
- [21] M. Bernhard and M. Schubert, “Robust object detection in remote sensing imagery with noisy and sparse geo-annotations,” in *ACM SIGSPATIAL*, 2022.
- [22] S. Ren *et al.*, “Faster r-cnn: Towards real-time object detection with region proposal networks,” *IEEE Transactions on Pattern Analysis and Machine Intelligence*, 2016.
- [23] T.-Y. Lin *et al.*, “Focal loss for dense object detection,” in *ICCV*, 2017.
- [24] Z. Tian *et al.*, “Fcos: A simple and strong anchor-free object detector,” *IEEE Transactions on Pattern Analysis and Machine Intelligence*, 2022.
- [25] K. He *et al.*, “Deep residual learning for image recognition,” in *CVPR*, 2016.
- [26] T.-Y. Lin *et al.*, “Feature pyramid networks for object detection,” in *CVPR*, 2017.
- [27] Y. Zhou *et al.*, “Mmrotate: A rotated object detection benchmark using pytorch,” in *ACM Multimedia*, 2022.
- [28] B. Wang, “A parallel implementation of computing mean average precision,” *arXiv preprint*, 2022.
- [29] C. Li *et al.*, “Instance-aware distillation for efficient object detection in remote sensing images,” *IEEE Transactions on Geoscience and Remote Sensing*, 2023.
- [30] V. Lalitha *et al.*, “A review on remote sensing imagery augmentation using deep learning,” *Materials Today: Proceedings*, 2022.
- [31] E. D. Cubuk *et al.*, “Autoaugment: Learning augmentation strategies from data,” in *CVPR*, 2019.
- [32] E. D. Cubuk *et al.*, “Randaugment: Practical automated data augmentation with a reduced search space,” in *CVPRW*, 2020.
- [33] D. Hendrycks *et al.*, “Augmix: A simple data processing method to improve robustness and uncertainty,” in *ICLR*, 2020.
- [34] Z. Wei *et al.*, “Amrnet: Chips augmentation in aerial images object detection,” *arXiv preprint*, 2020.
- [35] J. Han *et al.*, “You only cut once: Boosting data augmentation with a single cut,” in *ICML*, 2022.
- [36] D. Hendrycks *et al.*, “Pixmix: Dreamlike pictures comprehensively improve safety measures,” in *CVPR*, 2023.